POLITECNICO DI TORINO
Repository ISTITUZIONALE

Tall building structural analysis based on analytical formulation: a case study in Wenzhou, China

Original
Tall building structural analysis based on analytical formulation: a case study in Wenzhou, China / Lacidogna, G., Li, B., Silva Cezar, E., Jiang, Z., Jueliang, C.. - In: CURVED AND LAYERED STRUCTURES. - ISSN 2353-7396. - STAMPA. - 13:1(2026), pp. 1-19. [10.1515/cls-2025-0045]

Availability:
This version is available at: 11583/3012964 since: 2026-07-11T16:11:30Z

Publisher:
Walter de Gruyter

Published
DOI:10.1515/cls-2025-0045

Terms of use:

This article is made available under terms and conditions as specified in the corresponding bibliographic description in the repository

Publisher copyright

(Article begins on next page)

27 November 2026

Research Article

Giuseppe Lacidogna*, Bin Li, Ediblu Silva Cezar, Zihan Jiang and Jueliang Chen

Tall building structural analysis based on analytical formulation: a case study in Wenzhou, China

https://doi.org/10.1515/cls-2025-0045
Received September 10, 2025; accepted January 31, 2026;
published online July 2, 2026

Abstract: Tall buildings are complex structural systems that require efficient and accurate analysis methods, particularly during the early stages of design, when rapid decision-making is crucial. Although Finite Element (FE) modeling offers detailed insight into structural behavior, it often requires significant time and computational effort. In contrast, simplified analytical approaches can provide faster assessments with sufficient accuracy for preliminary design evaluations. This study applies an established analytical method, the so-called General Algorithm (GA), to assess the global dynamic response and the stress distribution of structural components of a 38-story high-rise building under wind-induced lateral loads, according to the Chinese standard (GB 50009-2012). The selected case study, located in Wenzhou, China, features an open shear-wall structural system with a regular cross sectional geometry. The analytical model yields results for displacements, natural frequencies, and mode shapes which show acceptable agreement with the original FE design documentation. A detailed stress analysis is conducted for a critical open shear-wall section, identifying the most stressed points and highlighting the influence of different stress components, including those described by Vlasov's theory. It was verified that axial and bending-induced stresses dominate the structural response, while the contribution of the warping effects was found to be minor. The study confirms that the GA formulation, despite its limitations, offers a practical and efficient tool for the preliminary structural assessment of tall buildings, especially in construction environments with a high demand for results in a short time, such as China nowadays.

Keywords: tall building; analytical formulation; stability analysis; Vlasov's theory

***Corresponding author: Giuseppe Lacidogna**, Department of Structural, Geotechnical and Building Engineering, Politecnico di Torino, Corso Duca degli Abruzzi, 24. 10129, Torino, Italy; and College of Architecture and Energy Engineering, Wenzhou University of Technology - Binhai Campus, Jinhai Third Road, 337, 325000, Longwan Economic and Technological Development Zone, Wenzhou, China, E-mail: giuseppe.lacidogna@polito.it
Bin Li, Zhejiang Lipeng Construction Company, Wenjin Road, Lucheng District 456, 325000, Wenzhou, China
Ediblu Silva Cezar, Department of Structural, Geotechnical and Building Engineering, Politecnico di Torino, Corso Duca degli Abruzzi, 24. 10129, Torino, Italy. https://orcid.org/0000-0002-4154-3189
Zihan Jiang, Department of Civil Engineering and Smart Cities, Shantou University, University Road 243, 515063, Shantou, China; and Department of Structural, Geotechnical and Building Engineering, Politecnico di Torino, Corso Duca degli Abruzzi, 24. 10129, Torino, Italy. https://orcid.org/0009-0002-5327-2512
Jueliang Chen, College of Architecture and Energy Engineering, Wenzhou University of Technology - Binhai Campus, Jinhai Third Road, 337, 325000, Longwan Economic and Technological Development Zone, Wenzhou, China

1 Introduction

The Council on Tall Buildings and Urban Habitat (CTBUH) [1] does not provide a precise or universal definition for a "tall building", as this classification depends on various factors, such as height relative to the surrounding context, construction technologies and other design considerations. Nevertheless, a building must be visually and functionally distinct within the urban landscape to be recognized as tall. Due to this distinctive presence, tall buildings have become enduring symbols of architectural modernization, as well as indicators of technological progress and economic growth in cities and regions around the world [2–7].

From an engineering perspective, numerical methods – particularly the Finite Element (FE) method – are well-established and powerful tools for analyzing complex structural systems, including high-rise buildings. FE analysis offers detailed insights into the global behavior of structures, enabling engineers and architects to explore a wide range of solutions that satisfy both architectural and structural requirements [8–12]. However, the extensive modeling effort required can be a limitation during the early stages of design. In the conceptual phase, multiple structural configurations are often explored, making rapid iteration essential. The preparation of detailed FE models is time-consuming and

Open Access. © 2026 the author(s), published by De Gruyter. This work is licensed under the Creative Commons Attribution 4.0 International License.

data-intensive, and the complexity of input/output information can sometimes obscure the fundamental structural mechanisms. This, in turn, may hinder a clear understanding of the force distribution and mechanical behavior of key structural elements, especially in a very complex build [13].

In this context, simplified analytical methods can serve as valuable tools during conceptual design. By relying on fewer variables, such methods allow for faster and more transparent modeling, reducing the likelihood of errors, and facilitating a clear interpretation of structural behavior. Although they may not match the precision of full FE simulations, analytical approaches can achieve sufficient accuracy for the preliminary evaluation of load-resisting mechanisms. Furthermore, by incorporating simplifying assumptions, they help identify critical structural parameters that can guide both early-stage decision-making and the development of subsequent FE models. Such analytical methods are particularly valuable for investigating stress distributions and dynamic behavior in complex or layered structural systems, highlighting the continued interest in efficient modeling techniques to evaluate deformation and internal forces.

Numerous analytical models have been developed to evaluate the mechanisms of lateral load resistance in tall buildings [14–20]. To address the wide variety of stiffening components and their unconventional arrangements in modern high-rise structures, this study adopts a generalized approach proposed by Carpinteri et al. [21, 22]. The analytical formulation presented here mainly aims to assess the global dynamic behavior of tall buildings under lateral wind loads. In addition to evaluating the dynamic response, this study also addresses the stress distribution in open shear-wall sections. Understanding the internal stress patterns in such structural elements is critical, particularly under lateral loads induced by wind or seismic forces, as these stresses directly influence the performance, durability, and safety of tall buildings. Accurate stress assessment allows for more efficient material use, better reinforcement details, and improved prediction of potential failure modes. By integrating both dynamic analysis and stress evaluation within an analytical framework, this work provides a comprehensive and efficient tool for the preliminary design and performance assessment of high-rise buildings, capable of capturing key stress and deformation patterns in regular and layered structural systems.

In this study, an established analytical formulation is employed to determine the stress distribution and vibration modes of tall buildings with open shear-wall systems under wind-induced lateral loads. It is important to clarify that the objective of this study is not to propose a new analytical formulation or to validate the existing GA method against detailed FE simulations. Instead, the main goal is to demonstrate its feasibility and usefulness as a practical tool to evaluate the structural behavior of high-rise buildings during the early stages of design, when comprehensive numerical models are not yet available. This applicability is particularly effective when the analyzed structure presents a section with regular geometry, as in the present case study.

Although the GA method has been validated by the authors and collaborators in European contexts?, [13], its application in conjunction with Chinese design codes (e.g., GB 50009-2012 for wind loads) remains less explored. This study aims to fill this gap by applying the GA formulation to a representative Chinese high-rise, assessing its performance under codified wind loads, and critically evaluating the significance of Vlasov's theory for warping stresses in a real-world design.

1.1 History of high-rise buildings in China

The history of tall building construction in China reflects the rapid economic development, technological advancements and the evolving urban modernization of the country [23]. Traditionally, China was known for its ancient architecture; however, with the country's transformation beginning in the late 20th century, the landscape of Chinese cities has undergone a dramatic change [24].

The emergence of tall buildings in China can be traced back to the 1980s and 1990s, coinciding with economic reforms and urbanization policies that spurred unprecedented growth in cities such as Shanghai, Beijing, Guangzhou and Shenzhen. These metropolises began to build iconic high-rise buildings to accommodate increasing populations, business needs, and the desire to showcase China's modernity on the world stage. Notable early examples include the Guangzhou Baiyun Hotel (~114 m – 1976) and the Guangdong International Building (~200 m – 1990) (see Figure 1(a)), which signaled the country's entry into the era of vertical urban development [25]. In the 21st century, China has become a global leader in tall building construction, with cities competing to build the tallest and most innovative structures. The development of "supertall" buildings, such as the Shanghai Tower – currently one of the tallest in the world – reflects advances in engineering, sustainable design, and architectural innovation [26]. China's high-rise boom is also driven by urban densification, economic aspirations, and the desire to create iconic cityscapes that symbolize modernity and progress. Today, the story of China's tall buildings is not only about reaching new heights, but also about integrating sustainable practices, smart technology, and cultural elements into urban architecture [27–29]. The evolution of these structures embodies the nation's journey

from ancient architectural traditions to cutting-edge urban development, making China a fascinating case study in the global history of high-rise structures.

Figure 1(a) shows the rapid progress in the tall building industry in China, with two iconic buildings from the end of the last century alongside modern constructions from the second decade of the 21st century. The Shanghai Tower (~678.9 m) holds the third position in the world ranking and is the tallest building in China and East Asia, containing entertainment areas, offices, and the highest luxury hotel in the world. Although Figure 1(b) encompasses the tallest buildings all over the world as of 2025, led by Burj Khalifa as the tallest building in the world since 2010, with an architectural height of ~828*m*.

To illustrate the representativeness of China on the global stage regarding the construction of tall buildings, Table 1 presents the top six countries listed by [1], ordered from those with the highest number of buildings considered tall (with +150 m height), for 2025. The list is led by China, which presents several tall buildings, with a total number of

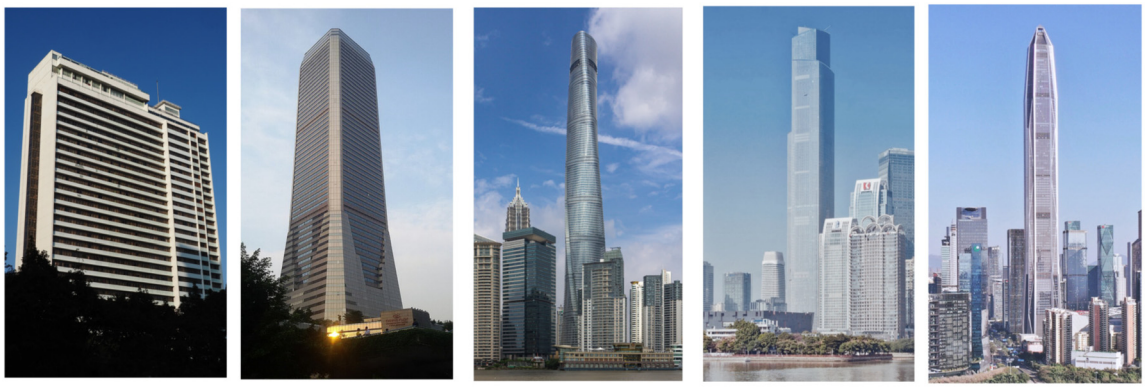

(a)

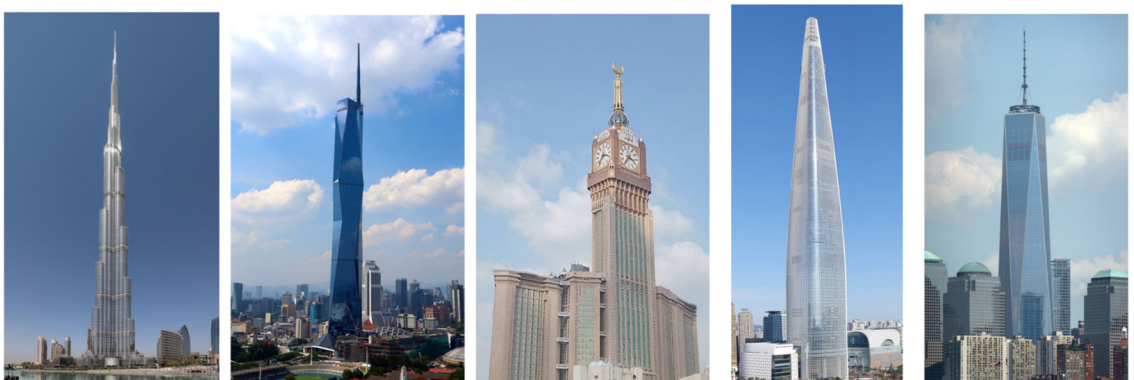

(b)

Figure 1: Development of tallest buildings (a) in China and (b) all over the world as of 2025. All the figures are under CC license.

Table 1: Countries with the highest number of tall buildings. Adapted from [1].

Rank	Country	Number of buildings			Tallest city
		150 m +	200 m +	300 m +	
1	CN	3,493	1,267	122	Hong Kong
2	USA	905	246	31	New York
3	UAE	342	158	37	Dubai
4	MY	319	73	6	Kuala Lumpur
5	JP	283	51	2	Tokyo
6	KR	281	80	7	Seoul

buildings around four times greater than the USA, in second place.

1.2 Overview of the tall building in Wenzhou, China

As mentioned above, high-rise building construction is expanding rapidly in different regions of China. In this scenario, we can mention Wenzhou City, Zhejiang Province, as an emerging city with constant growth and urban transformation. As shown in Figure 2(a), Wenzhou is located in a strategic position (extreme southeast of Zhejiang, bordering Lishui to the west, Taizhou to the north and Fujian province to the south), as the Sea coast in eastern China is a prolific area, regarding the construction of high-rise structures. According to [1], the first tall building built over 150 m in Wenzhou City was the China Telecom Building (156 m), in 1999, designated for office use. Also, according to [1], the current tallest building in the city of Wenzhou (with a status of Completed) is the Hilton Wenzhou City Center (339 m), 2024, with a function of hotel.

On the northeast side of Wenzhou City, in Oubei Street, Yongjia County, is the construction area of the building under study (see Figure 2(b)). It is located in this area as part of a future residential complex. The area is approximately 269,483.5 m^2, with a density of buildings of 37.1 % and a green space ratio of 35 % (for residential areas). The functional layout comprises residential units (110,346.6 m^2), commercial office spaces (97,000 m^2), and public facilities, including elderly care and cultural amenities.

This project is carried out and executed by the local Zhejiang Lipeng Construction Company, which possesses the following skills and expertise. The Zhejiang Lipeng Construction Company, established in 1997, holds top-tier qualifications in the China construction industry, including Grade I General Contracting for Construction Engineering. The company's business spans housing construction, landscaping, premium interior decoration, and municipal engineering. During the past five years, Lipeng Construction has achieved an average annual output value exceeding 6 billion RMB. Currently, the company manages more than 30 projects, with an annual construction area of approximately 5 million square meters. Recognized for excellence, the company has earned some awards, such as AAA Certification for Integrity, Safety, and Quality Management in China's Construction Industry, Standardized Demonstration Site of Zhejiang Province, and Green Construction Demonstration Project of Zhejiang Province. With a workforce of 1,200 employees, including 600+ technical professionals, the company has driven innovation in construction technology, securing multiple invention and utility model patents. It has been honored as a Zhejiang Technology-Based Enterprise and successfully designated as a Provincial Enterprise Technology Center. In particular, Li Peng Construction has shaped iconic landmarks in Wenzhou. An example of a building complex built by the Company can be seen in Figure 3(a).

Specifically, the K3-11 Project, which is made up of two towers, so called #1 and #2, see Figure 3(b). In this way, in this research paper as a case study, we evaluate the stability only of the tower #1, part of the K3-11 project, which is a 150 m high residential building (38 floors, including the ground floor) and is the tallest tower in the building complex currently in the final stages of construction in Wenzhou City.

As urbanization accelerates, high-rise buildings have emerged as a dominant trend in city development due to their efficient use of land. However, the associated issue of high energy consumption has also become increasingly prominent. From the planning stage, the K3-11 project has embraced the concept of green architecture, incorporating multiple energy-saving technologies to reduce operational energy consumption and enhance the environmental compatibility.

1.3 Green building design and environmental benefits

The case study is a 38-story (150 m) high-rise building in Wenzhou, located in a climate zone with hot summers and cold winters. In this context, a design that ensures effective summer heat insulation and winter warmth retention is required. The project adopts passive strategies, including adjustable shading systems, optimized natural ventilation, and a staggered building form to reduce cooling loads and enhance comfort.

The building envelope employs high-performance insulation materials (rock wool or graphite polystyrene



(a)

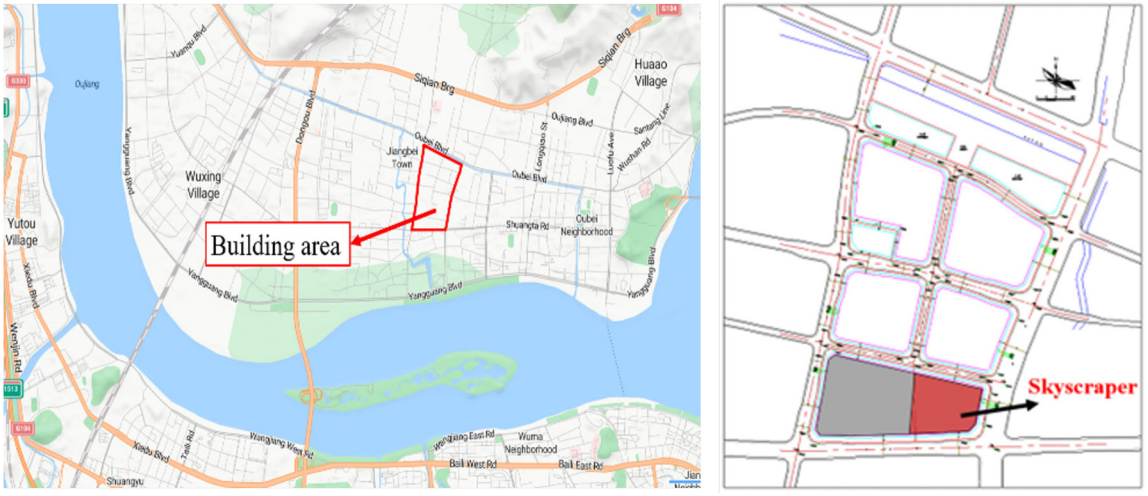

(b)

Figure 2: Location map: (a) Wenzhou city and (b) K3-11 project building area location.

boards, thermal transmittance ≤0.6/ (m^2K)) according to GB 50189. Double-glazed windows with Low-E (visible light transmittance ≥0.4, SHGC ≤0.5) combined with external shading devices minimize the solar heat gain. A lightweight green roof mitigates the urban heat island effect, while rooftop photovoltaic panels generate up to 120,000 k Wh annually, covering ~15 % of the public-area electricity demand. Rainwater harvesting achieves ≥10 % non-traditional water utilization for irrigation and road cleaning.

Sustainable materials are prioritized through the use of high-strength reinforcing steel and recycled concrete (≥30 % supplementary materials), along with prefabricated wall sections to reduce construction waste. These measures exceed national energy-savings standards by 25 %, resulting in an



(a)

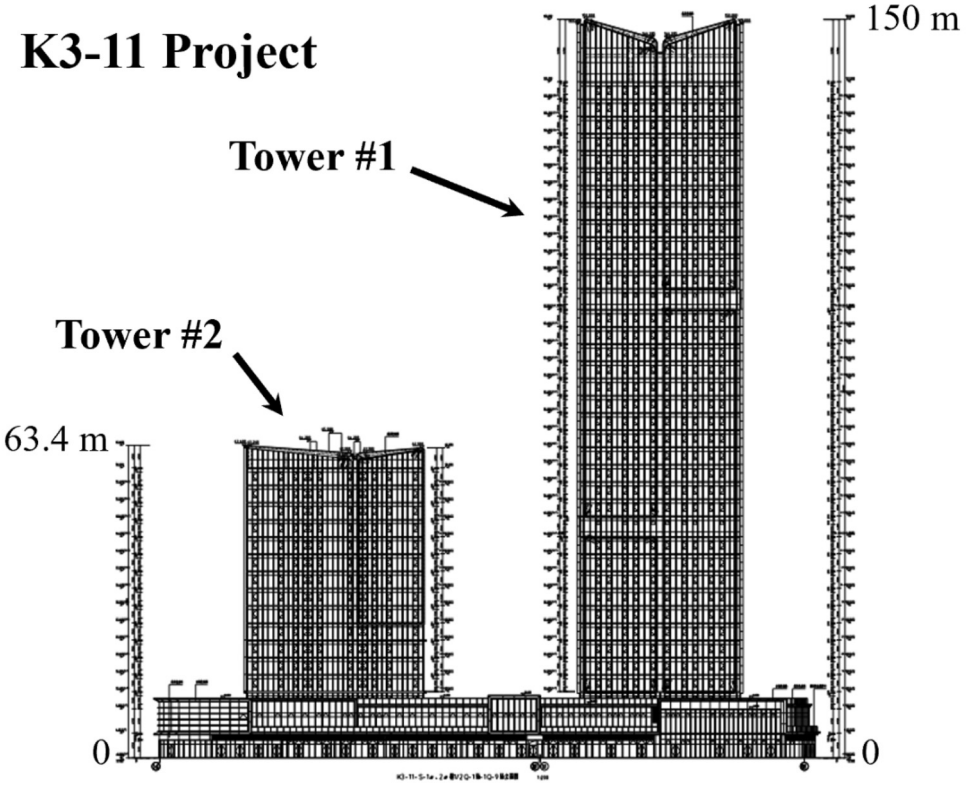

(b)

Figure 3: The double-tower building by Zhejiang Lipeng construction: (a) example of similar project carried out by the company and (b) side view of the K3-11 project.

estimated annual reduction in 1,200 t CO_2 emissions, with renewable energy accounting for more than 12 % of total consumption.

In addition to environmental performance, the project enhances social sustainability by providing 1,056 housing units, public cultural facilities (127 m^2), elderly care services (317 m^2), and 258 electric vehicle charging stations. Meeting the two-star requirements of the Green Building Evaluation Standard (GB/T 50,378), the building illustrates how integrated passive design, renewable energy systems, and sustainable materials can deliver high energy efficiency and environmental benefits in skyscraper projects.

2 Analytical model

As mentioned above, the case study comprises the analysis of a tower under construction (at the time of writing this work). The analyzed building is part of a residential complex in Wenzhou City, in China.

2.1 Building description

The case study structure, Tower #1 of the K3-11 project, is a high-rise reinforced concrete core–shear wall system composed of 38 functional floors (including the ground floor) and follows a regular structural scheme from the 3rd floor upward. The first two floors share the same plan dimensions as the rest of the tower but are surrounded by additional structural columns (Figure 4(b), which, for reasons of model simplification, are not considered in the present analysis.

The typical floor plan is rectangular, measuring 31.8 m along the north–south axis (x-direction) and 22.3 m along the east–west axis (y-direction). The layout is symmetric with respect to the y-axis, whereas in the orthogonal direction, the arrangement induces coupling between the flexural and torsional behavior under horizontal loading. With the exception of the refuge floors at levels 13 and 26 (each 4.2 m high), all floors of levels 3 to 38 have a story height of 3.5 m, resulting in a structural height of approximately 137.3 m up to the upper occupied floor. Above this, three non-functional floors form the roof structure, bringing the total height of the building to 150 m. The floor plan incorporates seven internal cores, all designed as open thin-walled sections and classified into four distinct types (Figure 4(c) and (d)). A single basement level (−1 floor) with a height of approximately 4.8 m houses service facilities and contributes to the condition of the building's fixed-base.

The entire building (coupling both towers) is designed for mixed-use occupancy, including residential and commercial spaces, in accordance with relevant Chinese design codes for loading, wind resistance, and seismic safety. Different concrete strength classes are used for vertical structural elements depending on elevation: concrete C70/85 for columns on the lower floors, C35/45 for upper floors, and C60/75 to C30/35 for the cores. In the present analysis, the effects of creep and shrinkage are neglected.

2.2 Analytical formulation

The general formulation used in this work is based on Capurso's approach [30], which was first proposed by A. Carpinteri [31]. The original computer program, written in Fortran®, analyzed structures with the limitation of containing $N_{TOT} \leq 20$ resisting elements, subject to Saint Venant's theory, and having up to $N \leq 30$ floors [31]. In recent years, the original Carpinteri formulation, known as the General Algorithm (GA), has been further developed and improved. It has been implemented in a Matlab®, computational code, initially incorporating Vlasov's theory for the calculation of open thin-walled sections [21], and later extending to analyze a broader range of high-rise building typologies ?, ?, [13, 22, 32, 33].

Now, the General Algorithm (GA) allows one to determine the distribution of external lateral load among vertical bracings, floor displacements, and the stresses acting on the vertical stiffeners of high-rise buildings without limitations. In the GA formulation, each vertical bracing is described within its own local coordinate system, with axes parallel to the principal directions of inertia and origin at the shear center of the section. All these vertical bracings are connected at each floor level by infinitely rigid slabs within their own plane, while being infinitely deformable outside the plane. These slabs can have closed and open thin-walled internal sections.

The basic formulation of the GA considers only three degrees of freedom (DOF) for each N-floor building, with N being counted from top to bottom. The unknown floor displacement vector $\{\delta\} = \{\{\xi\}; \{\eta\}; \{\vartheta\}\}$ consists of two translations along the x and y directions, respectively, and a rigid rotation around z-axis of the floors. The external $3N$-load vector applied to each floor $\{F\} = \{\{p_x\}; \{p_y\}; \{m_z\}\}$, is composed of the internal load vector $\{F_i\}$, which represents the concentrated loads acting in the x and y directions, and a plane torsional moment, applied to each i-th resistant element.

Moreover, as already mentioned, all geometric characteristics of the plane, including each vertical bracing, are localized by its own local reference system $x_i y_i$ (originating in the shear center of the plane and with axes parallel to the main directions of inertia), and therefore the local stiffness

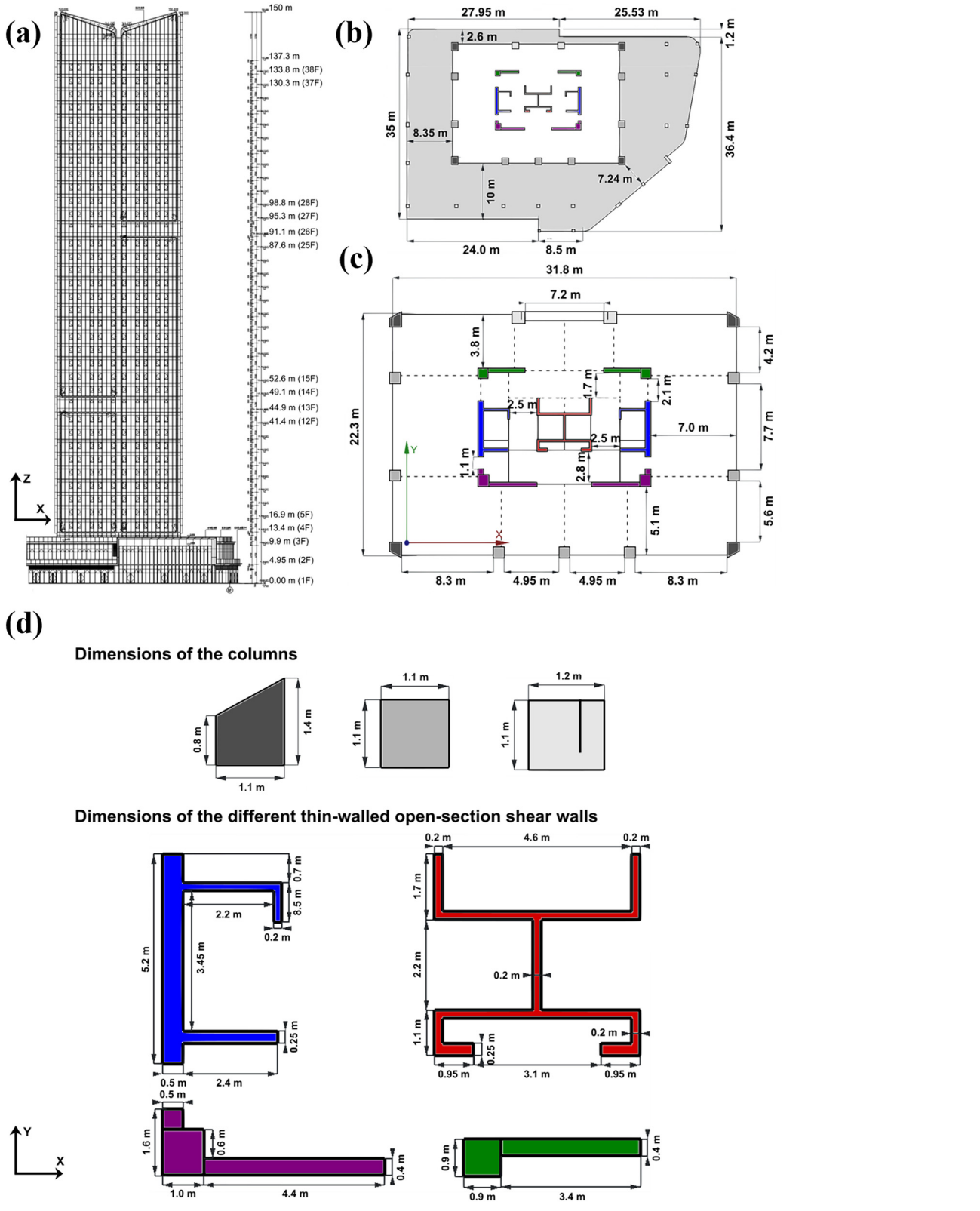

Figure 4: Structure description containing (a) lateral view of the K3-11 tower #1, (b) section dimensions for the 1, 2 floors, (c) section dimensions for the 3–38 floors and (d) structural components dimensions (columns and thin-walled open-section shear walls).

matrix $[\overline{K_i}]$ of the bracing refers to the local system $x_i y_i$. In this way, the internal loadings can be written as:

$$\{F_i\} = [\overline{K_i}]\{\delta\} \tag{1}$$

Thus, defining an arbitrary global reference system (in this case the origin is placed at the centroid of each floor with the axes parallel to the sides of the building), the global equilibrium equation allows the stiffness matrix of the entire building to be written as:

$$\{F\} = \sum_{i=1}^{M} \{F_i\} = \left(\sum_{i=1}^{M} [\overline{K_i}] \right) \{\delta\} = [\overline{K}]\{\delta\} \tag{2}$$

The vector of the forces acting on each bracing is obtained by means of the distribution matrix $[R_i]$

$$\{F_i\} = [\overline{K_i}][\overline{K}]^{-1}\{F\} = [R_i]\{F\} \tag{3}$$

when the vector $\{F_i\}$ is known. Inverting Eq. (1) determines the i-th rigid plane displacements $\{\delta\}$ and, therefore, the stresses acting on it. Details on the condensation procedure for the computation of the stiffness matrices have already been described in detail in previous work?, [31, 32].

For dynamic analysis, the entire building is modeled as an equivalent cantilever beam, in which the masses of the floors are concentrated in the gravity center of their own. In this way, the dynamic equilibrium equation of the system (in the absence of viscous dissipation) can be written in compact form as [33]:

$$[M]\{\ddot{\delta}\} + [K]\{\delta\} = \{0\} \tag{4}$$

where $[M]$ and $[K]$ are the mass and the stiffness matrix, respectively, and $\{\delta\}$ is the displacement vector. More details on the definition of the mass and stiffness matrix can be found in [33].

We assume from now on that the displacement vector $\{\delta\}$ is given by the product of a vector depending on the spatial coordinate $\{\zeta(z)\}$ and a scalar quantity depending on time $\{\psi(t)\}$, such as:

$$\{\delta\} = \{\zeta(z)\}\psi(t) \tag{5}$$

which allows us to rewrite Eq. (4) as:

$$[M]\{\zeta(z)\}\ddot{\psi}(t) + [K]\{\zeta(z)\}\psi(t) = \{0\} \tag{6}$$

The previous Eq. (6) leads us to an eigenvalue problem.

$$\det\left([K] - \omega_n^2 [M] \right) = 0 \tag{7}$$

where the terms ω_n are the angular frequencies of the system. In this way, it is possible to determine the $3N$ eigenvalues ω_n, from which the natural frequencies ($f_n = \omega_n / 2\pi$) and the periods of vibration of the building ($T_n = 1/f_n$) are derived. Once the n values of the angular frequencies are known, it is possible to determine the $3N$ eigenvectors $\{\zeta(z)\}$ that represent the deformed shapes of the building related to every mode of vibration [34].

2.3 Analytical model implications for the case study

For the case study, the previously described generalized analytical (GA) model is applied to evaluate the structural behavior of the K3-11 Tower #1, located in Wenzhou, China, which was in the final stages of construction at the time of this study. The main characteristics of the building and the floor plans are provided in Subsection 2.1 (see Figure 4).

The GA code requires the following input parameters:

i. Number of (functional) floors;
ii. Story height;
iii. Floor plan dimensions and geometry of structural components (frames and open shear-walls);
iv. Properties of the material of each structural component (Young's modulus E, Poisson's ratio ν and density ρ);
v. Concentrated wind load acting on each floor (kN).

To meet the requirements of the analytical formulation, the following simplifying assumptions are adopted:

(1) The thickness of the slab is constant along the height of the building (t = 0.15 m).
(2) Floors 1 and 2 are modeled with the same cross-section as floors 3 to 38; the peripheral columns shown in Figure 4(b) (gray section) are excluded from the analysis.
(3) All columns are modeled as rectangular prismatic members with uniform cross-sectional dimensions of 1.1 × 1.4 m.
(4) The columns are assumed to be equally distributed along each side of the floor plan.
(5) Story height is constant along the height of the building (h = 3.5 m).
(6) Each open shear-wall section (types 1–4) has a constant wall thickness ($b_{1,2,5,6}$ = 0.40 m; $b_{3,4,7}$ = 0.20 m) throughout the height of the building.
(7) The properties of the materials are assumed constant with height: C35/45 concrete ($E = 34 \times 10^6$ k Pa; ν = 0.18; ρ = 2,400 kg/m^3) for open shear-walls and C60/75 concrete ($E = 39 \times 10^6$ k Pa; ν = 0.18; ρ = 2,400 kg/m^3) for columns.

A perspective view of the model as well as its section is shown in Figure 5(a) and (b), respectively.

Figure 5 is just a visual representation, generated in Matlab®, of the simplified analytical model. However, it is worth having an easier visualization of the main considerations taken into account in the conception of the model,

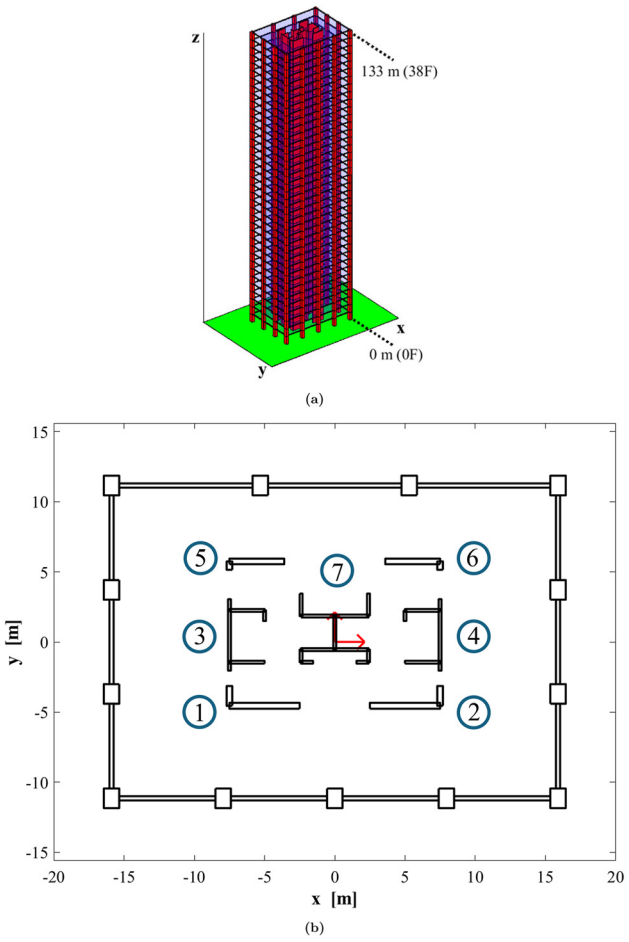

Figure 5: Visual representation of the (a) schematic diagram of the analytical model and (b) its floor plan.

such as the height considered (Figure 5(a)) and the constant space distribution between the columns on each side of the floor plan section (Figure 5(b)). The numbers in Figure 5(b) indicate the order in which each internal component (open shear-wall section) was inserted into the model. The frames were inserted in an anticlockwise direction, starting with the lower horizontal, vertical on the right, upper horizontal, and vertical on the left.

The assumptions described above define the geometric, material, and structural characteristics of the analytical model. The external lateral loading, represented by the wind action, is defined according to the Chinese Wind Load Code and is detailed in the following subsection.

2.4 Wind-load definition

The lateral loads acting on the building were determined in accordance with the Chinese Wind Load Code GB 50009-2012, as part of the original structural design documentation prepared by the local company design team (Zhejiang Lipeng Constr. Co.). In this study, an along-wind load is directly adopted from these original calculations and is depicted as concentrated wind forces applied at each floor level, ensuring consistency with the construction design of the project.

The design wind-load is based on a basic wind pressure of w_0 = 0.60 kN/m^2, corresponding to the regional wind climate. Taking into account the location of the building, a category C terrain (urban/suburban area) is considered. The values of the height coefficient $\mu_z(h)$ considering its variation along the elevation of the building are specified in Table 8.2.1 of GB 50009-2012.

The resulting concentrated wind forces applied to each floor level are shown in Figure 6. These loads are applied as discrete concentrated forces along the two principal axes (x, y) of the global coordinate system to assess structural response.

The higher concentrations of loads observed on the first floors of the building are a direct consequence of its larger area exposed to the effects of the wind, as previously shown in Figure 4(b), presented in the original project. In its upper part, the analytical model is a flat-roofed building. It should be noted that the wind load provided in the original design only includes lateral forces in the global x and y directions; no external torsional moment was considered. In this way, any torsional response observed in the analysis arises solely from the geometric and stiffness asymmetries of the building, rather than from applied load.

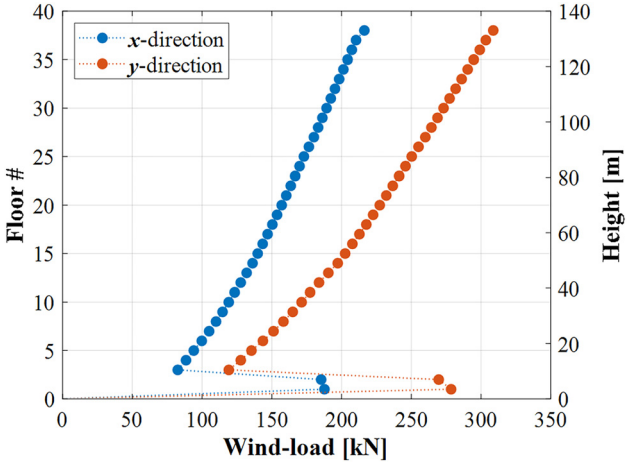

Figure 6: Applied wind-load forces distribution along the building height, based on GB 50009-2012.

3 Results and discussion

3.1 Global structural behavior

The global dynamic characteristics of the K3-11 Tower #1 were assessed by calculating its natural frequencies and vibration modes using the GA analytical formulation. In order to verify the analytical solutions, the results were compared with those obtained by the design team of the construction company. It is worth noting that all the results presented by the company, from its original project, were obtained using commercial Finite Element (FE) software SATWE2021(V1.4.0).

Table 2 presents a comparison of the first 10 natural frequencies and periods obtained by both approaches. The percentage change Δf(%) is calculated taking the numerical values as a reference. The comparison between the GA analytical model and the FE results indicates a Mean Absolute Percentage Error (MAPE) of approximately 11 %. While this deviation is not negligible, it is acceptable considering the intentional simplifications adopted in the GA formulation (uniform material properties, idealized cross-sections, omission of secondary stiffness contributions, etc.). From a computational perspective, each simulation required an average wall-clock time of approximately 10 s, with all computations performed on an Intel Core® i7-5500U CPU with 16 GB RAM. Thus, the analytical approach provides a transparent and computationally efficient alternative to complete FE analysis, while remaining sufficiently accurate considering the preliminary stages of the project.

In addition to the mode types presented in Table 2, Figure 7 illustrates the first four mode shapes, as 3-D perspective views, obtained from the GA model, as well as its correspondent floor plans. From Figure 7, it can be seen that the fundamental first mode corresponds to a prevailing lateral bending along the *x*-axis (north–south), followed by a coupled bending-torsion mode, with the bending occurring mainly along the *y*-axis. The third mode shape is predominantly torsional, and the fourth is prevailing bending along the *x*-axis, presenting two nodal sections.

The higher-order modes obtained follow the indication in the last column of Table 2, presenting coupled bending and torsional modes, as expected for a slender reinforced concrete high-rise structure. Finally, the vibration period obtained $T_1 = 1/f_1 = 5.4591$ s for the fundamental mode indicates that the building does not tend to be susceptible to

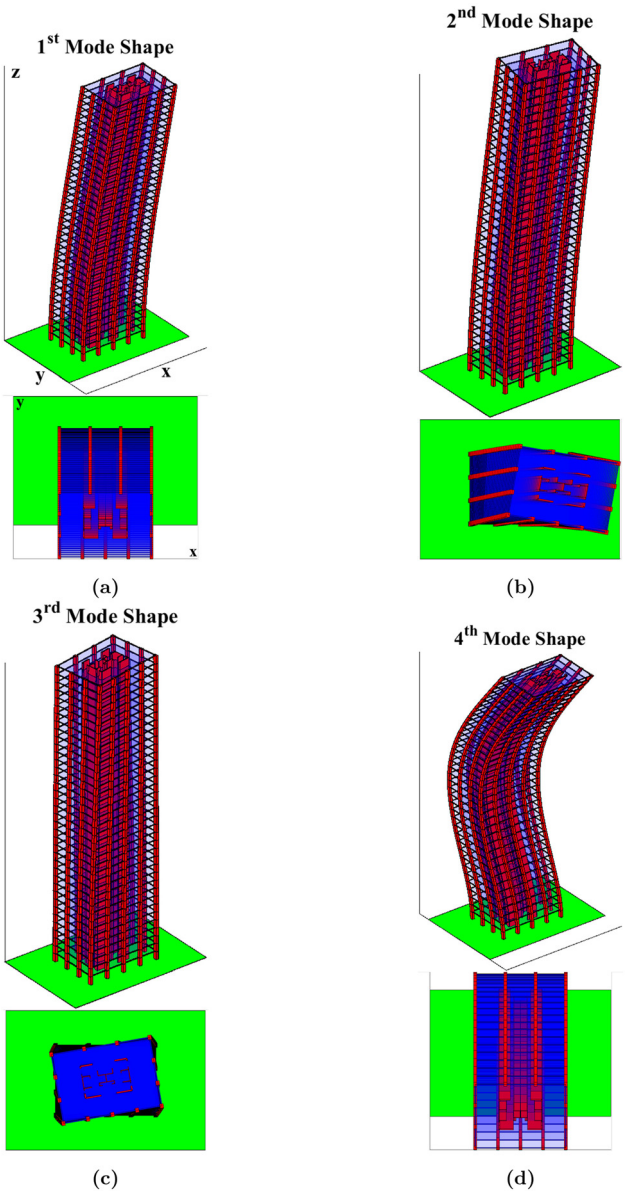

Figure 7: 3-D perspective views and floor plans of the first four vibration modes, (a) mode 1 (*Bx*), (b) mode 2 (*By* + *T*), (c) mode 3 (*T*) and (d) mode 4 (*Bx*).

Table 2: Comparison of natural frequencies between the analytical (GA) and numerical (FE) models.

Mode no.	Frequencies [Hz]		Difference Δf(%)	Mode type*
	Analyt. (GA)	Num. (FE)		
1	0.1832	0.25993	−29.5193	*Bx*
2	0.1892	0.27428	−31.0196	*By* + *T*
3	0.2694	0.38980	−30.8881	*T*
4	0.9331	0.90350	3.275508	*Bx*
5	0.9888	0.99910	−1.03101	*By* + *T*
6	1.1918	1.18976	0.17079	*T*
7	2.5049	1.73913	44.03175	*Bx*
8	2.669	2.06654	29.15291	*By* + *T*
9	3.0478	2.10172	45.01432	*T*
10	4.8605	2.64690	83.62969	*Bx*

**Bx*, bending about *x*; *By*, bending about *y*; *T*, torsional.

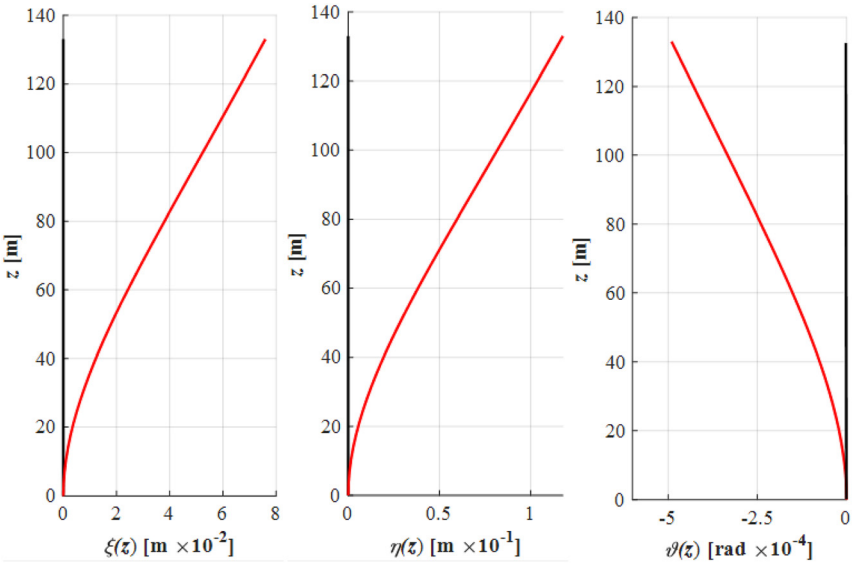

Figure 8: Displacement in x direction (ξ), displacement in y direction (η) and torsional rotation (ϑ).

the resonance effects of earthquakes (≈1 sec), that is, the most significant effects due to the action of the wind-load.

In addition to modal characteristics, the global displacement response under design wind loads (see Subsection 2.4) was evaluated (Figure 8). The GA model predicts maximum lateral displacements at the top floor (38th) of ξ = 0.07597 m in the x-direction and η = 0.11760 m in the y-direction, which are of the same order of magnitude as those obtained from the FE analysis (ξ_{FE} = 0.08607 m and η_{FE} = 0.13817 m). Furthermore, the GA model provides an estimate of the global torsional rotation around the vertical z-axis, yielding a value of $\vartheta = 4.904 \times 10^{-4}$ rad at the 38th floor, which cannot be identified from the output of the FE model. It should be emphasized that the purpose of this work is not to validate the analytical formulation against FE results but rather to illustrate that such a simplified analytical approach can deliver consistent results with more detailed simulations. Therefore, this demonstrates its potential as a reliable and efficient tool in the early stages of structural design, when a full FE model may not yet be available.

3.2 Contribution of the structural components

The contribution of each structural component to the global lateral resistance was quantified by comparing the total forces resisted by each element with the overall response of the building in both global directions (x and y) and is shown in Figure 9.

From Figure 9, it can be seen that not all components contribute equally. Some elements, such as (central) open shear-wall (OSW) 7, provide the largest share of global stiffness, carrying about 31 % of the total resistance in the x-direction and 25 % in the y-direction. Other components (e.g. OSW 1, 2 and the lower (LH) and upper (UH) horizontal frames) provide moderate contributions ranging between 5 % and 15 % depending on the axis. By contrast, the right (VR) and left (VL) vertical frames contribute almost exclusively in the y-direction, while their x-direction share is negligible.

We can highlight the small negative percentages of OSW 1 and OSW 6, for the y-direction. These can be associated with local redistribution effects and sign conventions in the global system: rather than resisting the global displacement, such elements slightly release or transfer load to the other components. However, their absolute values remain negligible compared to the dominant contributions.

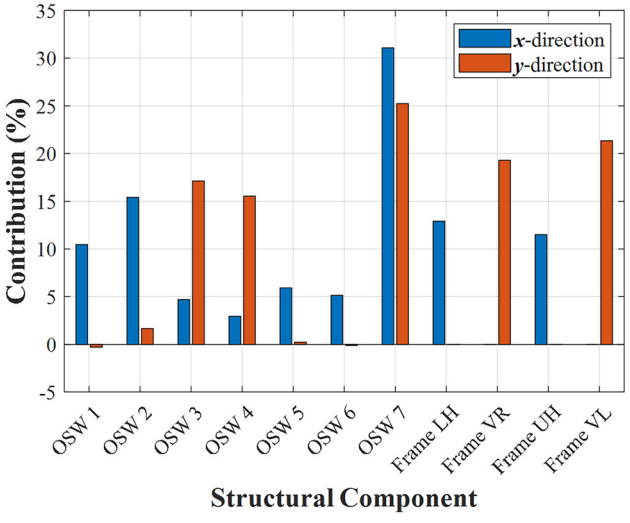

Figure 9: Component contributions to lateral resistance.

The results confirm that the lateral resistance is not uniformly shared, but is instead concentrated in a few key structural components, with OSW Section 7 playing a central role in both directions. This uneven distribution is in agreement with the Fazlur Khan's concept of 'premium for height', which explains why certain elements must contribute disproportionately to stiffness as tall structures become more slender [35], with shear walls typically dominating lateral resistance and frames acting as a complement. These findings reinforce the importance of carefully considering component geometry and placement, as overall structural stability and stiffness depend critically on a limited number of components.

3.3 Stress distribution in open shear-wall section

As shown in Subsection 3.2, the lateral resistance of the building is not uniformly shared among its structural components. The open shear-wall OSW-7 was identified as the component that provides the largest contribution to global lateral resistance in both directions (≈31 % in x and ≈25 % in y), making it the most representative internal core for detailed stress assessment. Focusing on OSW-7 therefore captures the critical demand paths governing global drift control and torsional coupling of the structure.

3.3.1 Geometric properties and internal resultants

Figure 10(a) shows the midline of the thin-walled OSW-7 section indicating the numbering vertex adopted for the stress analysis, as well as the location of its gravity center (red dot) and shear center (light-blue dot), both obtained related to the global reference system. Vertices 3 and 4 are located in the symmetric vertical axes. The sectorial area (ω_C) is calculated considering the shear center (C) as the pole and the vertex 1 as the sectorial origin. The sectorial area is positive when the radius vector rotates clockwise and is negative when the radius vector rotates counterclockwise. The distribution of the sectorial area (ω_C) for each vertex of the current section can be seen in Figure 10(b).

Table 3 summarizes the main geometric properties used by the GA analytical formulation to calculate stress.

The GA formulation is capable of providing the internal reactions for each internal core (close or open thin-walled section), considering a local and global reference system along the height of the building. Focusing on the issue of warping in the open thin-walled sections, the Vlasov's theory is applied to determine the primary torsional moment (M_z^{SV}), the secondary torsional moment (M_z^{VL}), and the bimoment (B) acting on each internal core, respectively, through the following equations ?:

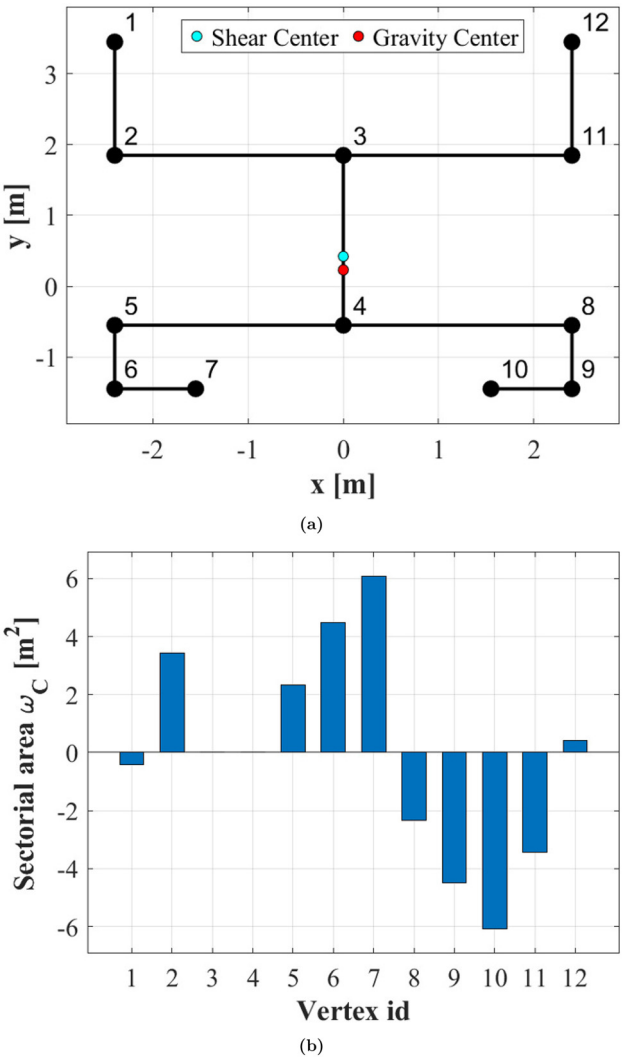

Figure 10: Geometric details of OSW-7: (a) middle line section and (b) sectorial areas of its vertices.

Table 3: Geometric properties of the OSW-7.

Property	Symbol	Value	Unit
Cross-section area	A	3.74	m^2
Wall thickness	b	0.2	m
Number of floors	–	38	–
Centroid coordinates	(x_G, y_G)	(0.00, 0.23)	m
Shear center coordinates	(x_C, y_C)	(0.00, 0.42)	m
Moments of inertia	$J_x; J_y$	11.26; 16.06	m^4
Product of inertia	J_{xy}	0.00	m^4
Warping constant	J_ω	11.30	m^6
Torsional rigidity	J_t	0.0784	m^4

$$M_z^{\mathrm{SV}} = GJ_t\vartheta' \tag{8a}$$

$$M_z^{\mathrm{VL}} = \frac{d}{\mathrm{d}z}B = -EJ_\omega\vartheta''' \tag{8b}$$

$$B = -EJ_\omega\vartheta'' \tag{8c}$$

where ϑ is the rotation of the floor, J_t the torsional stiffness factor of the internal core section under analysis, and J_ω indicate the sectorial moment of inertia. E and G represent the axial and tangential modulus of elasticity of the core material, respectively.

Taking into account the OSW-7 section under analysis, and its local reference system, Eq.(8) was used to calculate the reaction distribution along the height of the total torsional moment $M_z^{\mathrm{Total}}(z) = M_z^{\mathrm{SV}} + M_z^{\mathrm{VL}}$ and bimoment $B(z)$. The results can be seen in Figure 11(a) and (b), respectively. The null primary torsional moment (M_z^{SV}) at the base is a direct consequence of the boundary conditions of the analytical formulation, which says the base is constrained, preventing its warping ($\vartheta' = 0$). In addition, the same consideration makes the bimoment $B(z)$ present a maximum value at the base and be null at the free end of the structure.

It is worth noting that since no external moment was initially applied, the total torsional moment $M_z^{\mathrm{Total}}(z)$ is only a consequence of the horizontal wind load applied in the principal x and y directions. It is yet worth noting that, in addition to the internal reactions plotted in Figure 11, the GA formulation also provides the internal reactions M_x, M_y, T_x and T_y (not plotted here), always considering the local reference system of the analyzed section.

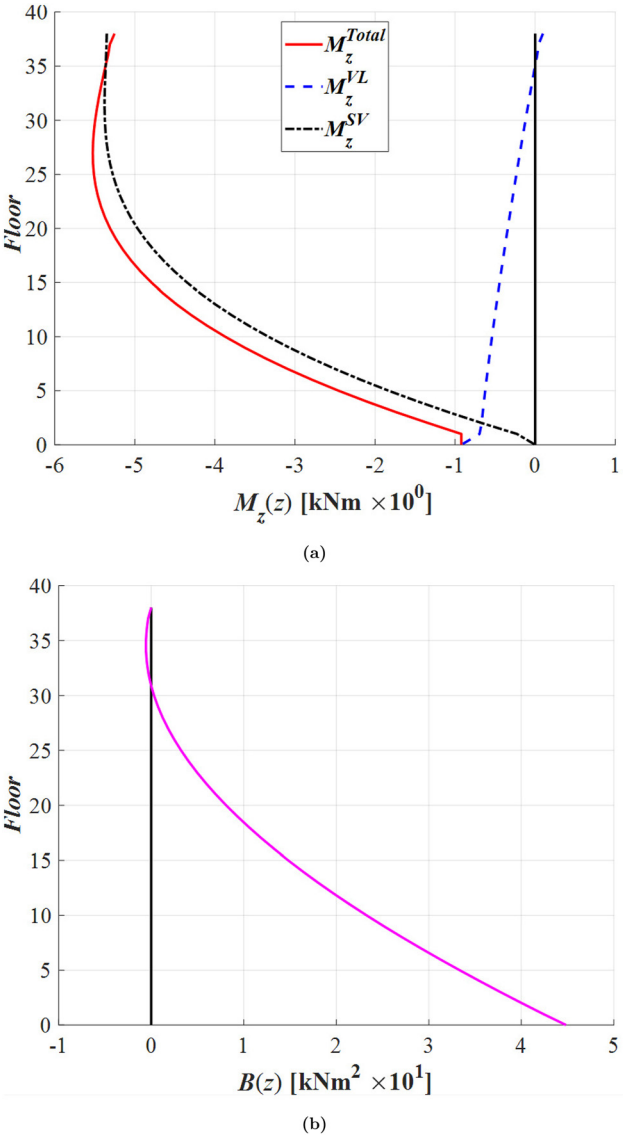

Figure 11: Internal reactions (a) torsional moment $M_z(z)$ and (b) bimoment $B(z)$ acting on OSW-7.

3.3.2 Stress distribution and critical regions

The generalized axial/normal stress (σ_z) based on the corresponding internal reactions, acting on the analyzed section, is obtained by the following equation:

$$\sigma_z = \sigma_z^{\mathrm{SV}} + \sigma_z^{\mathrm{VL}} = \left(\frac{M_x}{J_x}y + \frac{M_y}{J_y}x\right)^{\mathrm{SV}} + \left(\frac{B}{J_\omega}\omega\right)^{\mathrm{VL}} \tag{9}$$

where M_x and M_y indicate the bending moment related to the x and y axes, respectively. B is the bimoment, J_x and J_y indicate the moments of inertia, and ω is the sectoral area of the section. As indicated in Eq. (9) part of normal stress comes from Saint-Venant's theory (σ_z^{SV}), based on the hypothesis of plane section, while the other appears due to out-of-plane warping of the open thin-walled section (σ_z^{VL}), named Vlasov's theory.

Regarding generalized tangential stresses (τ_z) the following equation can be used [32]:

$$\tau_z = \frac{1}{b}\left[\frac{T_x}{J_y}S_y(S) + \frac{T_y}{J_x}S_x(S) + \frac{M_z^{\mathrm{VL}}}{J_\omega}S_\omega(S)\right] \tag{10}$$

where b is the thickness of the wall and S is the midline of the section. S_x and S_y are static moments and S_ω is the sectorial static moment. The T_x and T_y are shear internal forces and M_z^{VL} is the secondary torsional moment. Similarly to normal stress, tangential stress also presents two components, one derived from Jourawski's theory (first two terms) and the other derived from Vlasov's theory (last term). For more details on the derivation of Eq. (10), see reference [32].

In this way, the GA formulation allows floor-by-floor calculation of normal stress σ_z due to axial forces and

bending moments, and tangential stress τ_z due to torsion and shear forces, at each vertex of the analyzed section, allowing the identification of critical regions/points. It should be noted that the contribution of dead load (by structural self-weights) is not considered in this study.

Taking into account the OSW-7 under analysis, Table 4 summarizes the maximum intensity of each component of both normal and tangential stresses. For normal stress σ_z the intensity Max and Min indicates whether it is tensile or compression stress. It is also indicated in Table 4, the floor number and the vertex id, at which each extreme stress value occurs.

It can be highlighted that, except for $\tau_z^{\text{jourawski}}$, which maximum occurs on floor number 2, all the other components have maximum intensity on the bottom floor (1), as expected. Regarding the vertex, the maximum tensile value occurs on vertex 12, while the compression appears on vertex 6 of the section. In addition, the maximum intensity of the tangential stress is pointed in vertex 3 of the section.

Based on the results reported in Table 4, the stress intensity acting in section OSW 7 is plotted in Figure 12, on the 1st floor, which is considered the most critical. The behavior of each component of normal and tangential stress can be seen, according to Eq. (9) and Eq. (10), respectively. According to Table 4 the highest compression and normal tensile stresses can be verified in vertices 6 and 12, respectively (Figure 12(a)). Furthermore, other vertices also present relatively high levels of normal stress, i.e., vertices 5, 7 (both in compression) and 11 (in tensile), indicating the critical regions of the section for normal stress. At this level, the contribution of the bimoment $\left(\sigma_z^{\text{VL}} = \frac{B}{J_\omega}\omega\right)$ is negligible for any vertex of the section, compared to the stress levels arising from bending moments (M_x, M_y).

Regarding tangential stress τ_z, for the 1st floor level, the vertices that present the highest intensity are 3, 4, and 10, followed by 5 and 11 (Figure 12(b)). Indeed, vertices 3 and 4 are located on the symmetric vertical-axis and present the same tangential stress intensity, as vertex 3 is pointed out in Table 4. It is also interesting to note that vertices 1 and 12 do not experience any effect of tangential stress along the height of the building (see Figure 12(b)). This happens due to the sequence adopted for the vertices of the section, which computes zero static moments and sectorial moments for these vertices.

As well as for normal stress, for tangential stress, the contribution of the secondary torsional moment $\left(\tau_z^{\text{VL}} = \frac{1}{b}\left[\frac{M_z^{\text{VL}}}{J_\omega}S_\omega(S)\right]\right)$ is quite negligible for all vertices, at this level, being its maximum contribution to vertex 7, as previously indicated in Table 4.

As noted in Table 4, as well as in Figure 12(a), vertices 6 and 12 are critical considering normal stress, related to its

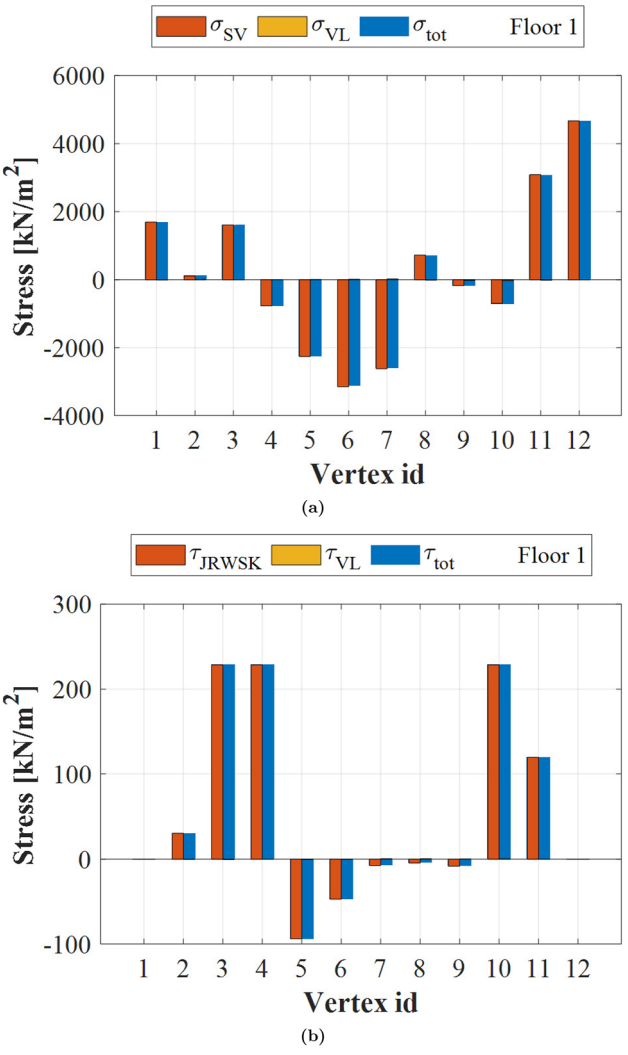

Figure 12: OSW-7 stress components (a) normal σ_z and (b) tangential τ_z stress components acting on OSW-7, on the 1st floor level.

Table 4: Global critical stress points of OSW-7.

Stress	Intensity	Value [Mpa]	Floor #	Vertex id
σ_z^{tot}	Max	4,992.616	1	12
	Min	−3,345.846	1	6
σ_z^{SV}	Max	4,990.997	1	12
	Min	−3,363.651	1	6
σ_z^{VL}	Max	24.112	1	7
	Min	−24.112	1	10
$\lvert\tau_z^{\text{tot}}\rvert$	Max	229.190	1	3
$\lvert\tau_z^{\text{jourawski}}\rvert$	Max	228.657	2	3
$\lvert\tau_z^{\text{VL}}\rvert$	Max	0.845	1	7

intensity. Therefore, the distribution of its normal stress components along the floors/height is shown in Figure 13(a) and (b), respectively. Due to their different magnitudes, all stress distributions were scaled by the maximum absolute value, resulting in normalized values within the interval [−1, 1]. The global normalization procedure preserves the stress sign, ensuring the physical distinction between compression and tension. The adopted normalization therefore facilitates a direct and unbiased comparison of their behavior along the structure height. In this regard, Figure 13 also shows that normal stress (σ_{SV}) changes its signal at the same point (specifically between floors 26 and 27) for both 6 and 12 vertices, while the bimoment component (σ_{VL}) remains similar with respect to its sign. Furthermore, the absolute values of the component (σ_{VL}) are very low for both vertices, compared to the intensity of the stress components σ_{SV} (indicated in Table 4), i.e., σ_{VL} = 17.8057 M Pa for vertex 6 and σ_{VL} = 1.6187 M Pa for vertex 12, at the 1st floor level.

Making reference again to Table 4 and Figure 12, the previous idea is applied to vertices 3 and 7, regarding the tangential stress component, and its behavior can be seen in Figure 14(a) and (b), respectively. Once again, due to its magnitude differences, the stress distributions were scaled by the maximum absolute value, resulting in normalized values within the interval [−1, 1]. The difference between its intensities is clear, as the tangential stress presents a more irregular behavior, either in relation to the vertices on each floor or along the height.

The very small difference between τ_{SV} and τ_{tot}, in Figure 14(a), demonstrates the small contribution of the

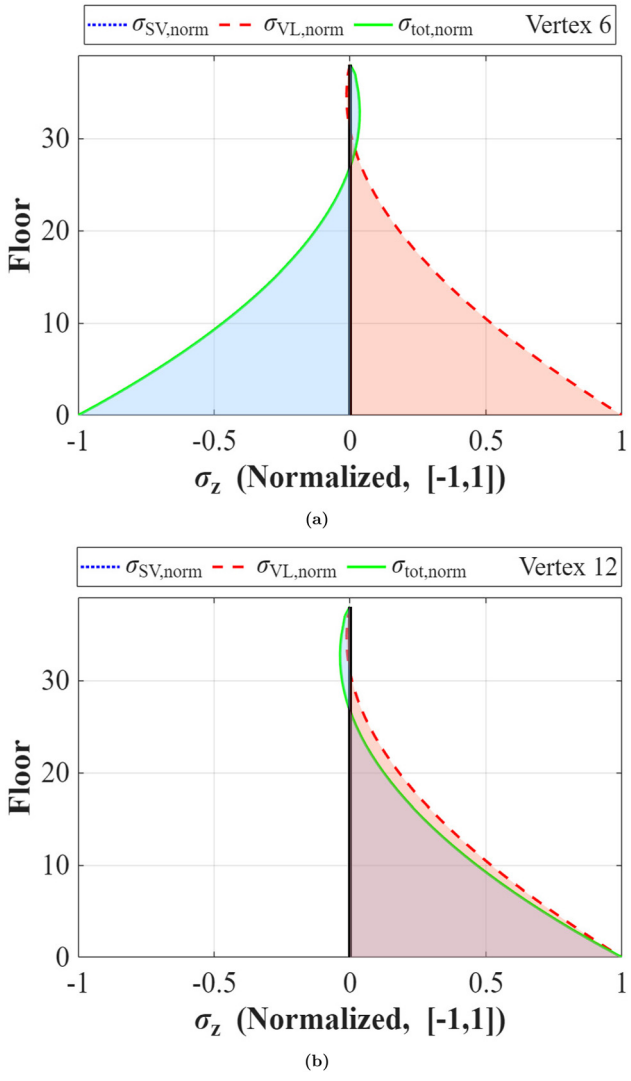

Figure 13: Distribution of normal stress components (σ_z) along the floors/height for vertices (a) 6 and (b) 12.

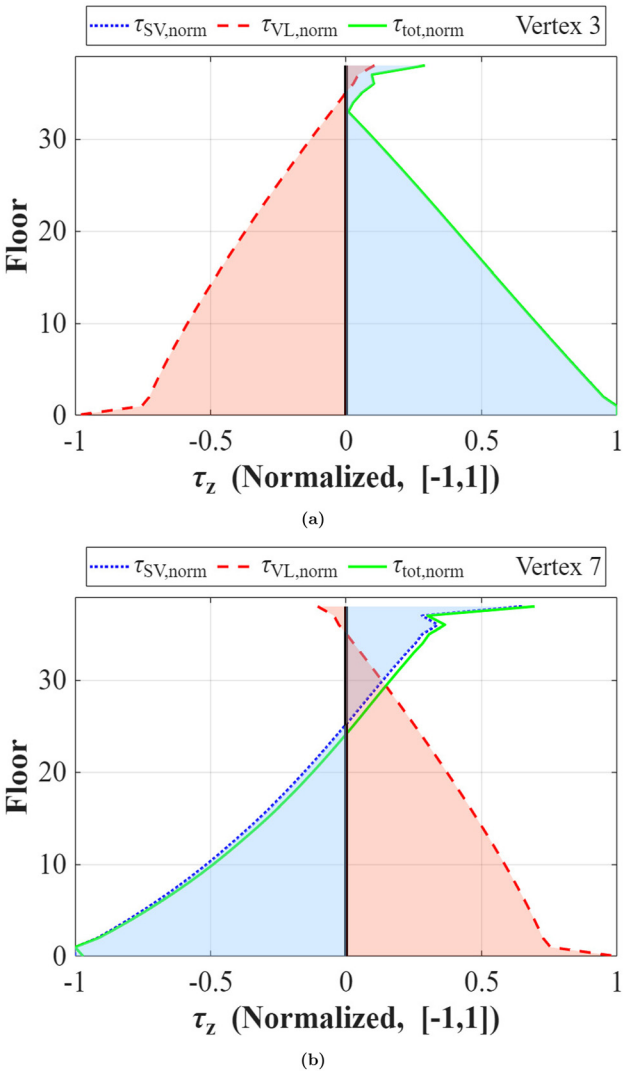

Figure 14: Distribution of tangential stress components (τ_z) along the height for (a) 3 and (b) 7 vertices.

secondary torsional stress component (τ_{VL}), exactly $|\tau_{VL}|$ = 0.5334 M Pa, on floor 1, for vertex 3. Although Figure 14(b) shows a relatively sensible difference between τ_{SV} and τ_{tot}, which indicates the contribution of the τ_{VL} component for vertex 7 ($|\tau_{VL}|$ = 0.8446 MPa), as indicated in Table 4.

3.3.3 Remarks about Vlasov components contributions

The most significant contribution of the Vlasov's theory-based component [21, 36] to normal stress (σ_z), acting on the open shear-wall Section 7 (analyzed) is shown in Figure 15.

After carefully analyzing all floors and vertices, it was found that the most significant participation of σ_z^{VL} occurs at the vertex 10, 25 floor, as shown in Figure 15(a). At this vertex, 70.93 % of the σ_{tot} value is due to bimoment contribution. Other relevant contributions can be pointed out:

- Vertex 6, floor 27 (20.24 %);
- Vertex 11, floor 27 (19.2 %);
- Vertex 10, floor 26 (10.59 %).

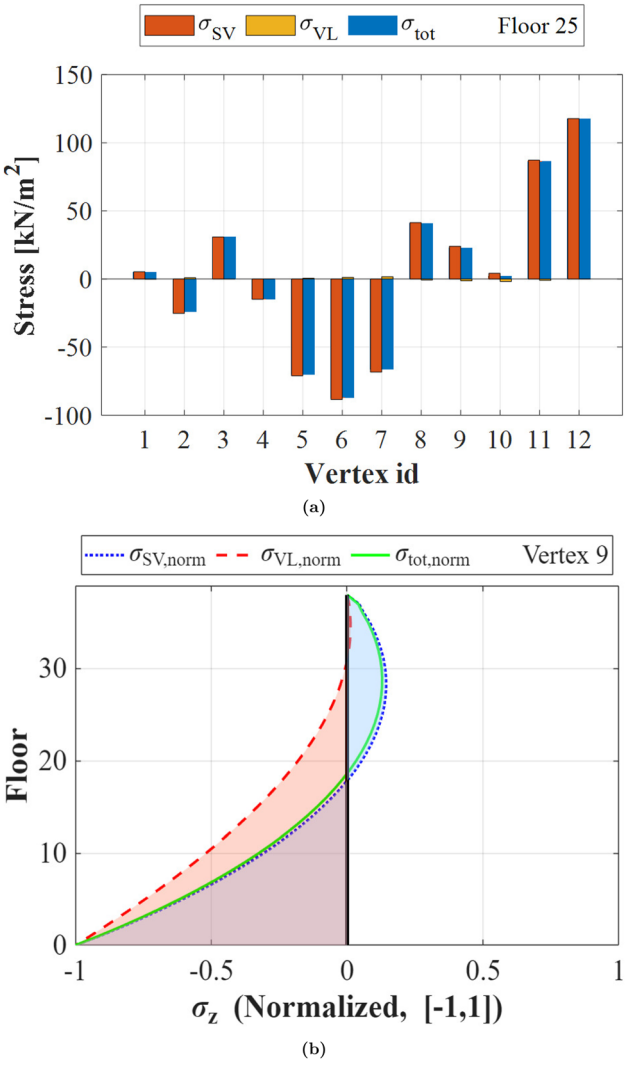

Figure 15: Normal stress (σ_z) components on section (a) at floor 25 and (b) along the height for vertex 9.

Although the main contribution of σ_z^{VL} related to σ_{tot} along the height was found for vertex 9 (8.69 %), being the highest in the bottom and the lowest in the top, as shown in a normalized graph, in Figure 15(b). However, in this case, the stresses induced by warping do not have much influence on the global normal and tangential stresses. This can be related to the geometry of the case study, which is quite regular, avoiding the effects of asymmetries, and thus limiting the torsional effects.

Despite its lower values in the analyzed section of the case study presented in this work, Vlasov's theory is still crucial, when open thin-walled sections are considered, especially in the early stages of the project, while this kind of analyzes performed with the GA analytical formulation can quickly define with good agreement, the geometry (thickness, size, shape) and the position in the floor section of each structural element.

4 Conclusions

Using the so-called General Algorithm (GA) analytical formulation, this paper analyzes a case study of a high-rise building currently under construction in Wenzhou, China. The GA was first introduced by Carpinteri et al. [31] and subsequently extended to incorporate Vlasov's theory for the calculation of thin-walled open sections [21], as well as to analyze a broader range of high-rise building typologies ?, ?, [13, 22, 32, 33]. The purpose of this approach is to investigate the structural behavior of braced high-rise systems, evaluating the method's accuracy and effectiveness.

The case study comprises a 38-story high-rise tower, part of the K3-11 project, subjected to horizontal wind-loading. The lateral loads that act on the building were determined in accordance with the Chinese Wind Load Code GB 50009-2012, as part of the original structural design documentation. An analytical model was created, and displacements, natural frequencies, and mode shapes were evaluated.

Since the GA formulation is already well established, the objective of this work is not to validate its solutions but to demonstrate that its results – such as top displacements and natural frequencies – show a feasible agreement with those obtained from the finite element (FE) analysis of the original project.

The analysis of global behavior identified an open shear-wall section (named OSW-7) as the critical structural element. Its geometry was characterized through vertices and sectorial properties, allowing a detailed stress analysis that considered the contributions of each component to normal and tangential stresses acting on the section. Vertices 6 and 12 were found to be critical with respect to normal stress (excluding dead load effects), while vertices 3 and 7 were more susceptible when tangential stresses were considered. In both cases, the bottom floor (Floor 1) was identified as the most critical. Additionally, given the configuration of the open thin-walled section, particular attention was paid to stress components following Vlasov's theory. However, the contribution of these warping-related stresses was relatively low compared to those from axial forces and bending moments.

In conclusion, despite its inherent limitations, the GA analytical method proves effective for analyzing high-rise buildings with regular cross-sections. The approach offers a transparent and computationally efficient framework, which makes it particularly suitable for preliminary design stages and rapid decision-making processes. This is especially relevant in contexts such as contemporary China, where accelerated construction schedules often require reliable but simplified analytical tools.

With regard to potential extensions, future research could investigate the applicability of the GA formulation to structures with irregular cross-sections or hybrid structural systems. Such extensions may be achieved through piecewise idealization of non-uniform geometries, equivalent stiffness representations, or coupling with reduced-order numerical models. Furthermore, the formulation could be expanded to account for different wind loading conditions, including crosswind, moment-induced, and torsional effects. In this context, integration with data-driven or machine learning techniques may further enhance the capability of the GA approach for rapid parametric studies and preliminary optimization tasks.

Acknowledgments: The authors thank Zhejiang Lipeng Construction Company for providing the material needed to carry out this work. The authors are also grateful to the reviewers for their valuable comments, which helped improve the manuscript.

Research ethics: Not applicable.

Informed consent: Not applicable.

Author contribution: All authors have accepted responsibility for the entire content of this manuscript and approved its submission. GL: Writing – review & editing, Methodology, Investigation, Data curation, Conceptualization. BL: Investigation, Data curation, Methodology. ESC: Writing – original draft, Methodology, Investigation, Formal analysis, Data curation, Conceptualization. ZJ: Writing – review & editing, Methodology, Investigation, Conceptualization. JC: Methodology, Investigation, Conceptualization.

Use of Large Language Models, AI and Machine Learning Tools: None declared.

Conflict of interest: The authors state no conflict of interest.

Funding information: This work was supported by the China National Global Excellent Scientists Fund 2025, the China Scholarship Council (CSC), and the basic research funds provided by Politecnico di Torino, Italy.

Data availability statement: The data supporting this study are available from the corresponding author upon reasonable request.

References

1. The Council on Vertical Urbanism (CVU). Tall building criteria – CTBUH. https://www.ctbuh.org/resource/height.
2. Mostafavi F, Tahsildoost M, Zomorodian ZS. Energy efficiency and carbon emission in high-rise buildings: a review (2005-2020). Build Environ 2021;206:108329.
3. Nugroho NY, Triyadi S, Wonorahardjo S. Effect of high-rise buildings on the surrounding thermal environment. Build Environ 2022;207:108393.
4. Kim JY, Park CY, Lee DK, Yun SH, Hyun JH, Kim ES. The cooling effect of trees in high-rise building complexes in relation to spatial distance from buildings. Sustain Cities Soc 2024;114:105737.
5. Forcellini D, Kalfas KN. Inter-story seismic isolation for high-rise buildings. Eng Struct 2023;275:115175.
6. Tominaga Y, Shirzadi M. Wind tunnel measurement of three-dimensional turbulent flow structures around a building group: impact of high-rise buildings on pedestrian wind environment. Build Environ 2021;206:108389.
7. Ali Memon S, Zain M, Zhang D, Rehman SKU, Usman M, Lee D. Emerging trends in the growth of structural systems for tall buildings. J Struct Integrity Maint 2020;5:155–70.
8. Kim H-S, Lim Y-J, Lee H-L. Optimum location of outrigger in tall buildings using finite element analysis and gradient-based optimization method. J Build Eng 2020;31:101379.
9. Avci O, Alkhamis K, Abdeljaber O, Alsharo A, Hussein M. Operational modal analysis and finite element model updating of a 230 m tall tower. Structures 2022;37:154–67.
10. Cai K, Huang M, Wang C, Yang C, Ni Y-Q, Li B. A combined approach to estimate modal parameters for updating the finite element model of a high-rise building. Struct Control Health Monit 2024;2024:3650202.
11. Wang Y, Zhao D, Li H. Finite element model updating technique for super high-rise building based on response surface method. Buildings 2025;15:126.
12. Qi Z, Li Q-S, Lu B. Reconstructing displacements of high-rise buildings during typhoons using machine learning with finite element method. J Build Eng 2025;108:112815.

13. Carpinteri A, Lacidogna G, Cammarano S. Structural analysis of high-rise buildings under horizontal loads: a study on the intesa Sanpaolo Tower in Turin. Eng Struct 2013;56:1362–71.
14. Hoenderkamp JCD, Snijder HH. Approximate analysis of high-rise frames with flexible connections. Struct Des Tall Build 2000;9:233–50.
15. Lee J, Bang M, Kim J-Y. An analytical model for high-rise wall-frame structures with outriggers. Struct Des Tall Special Build 2008;17: 839–51.
16. Kim HS, Lee DG. Analysis of shear wall with openings using super elements. Eng Struct 2003;25:981–91.
17. RaphaëlSteenbergen DJM, Blaauwendraad J. Closed-form super element method for tall buildings of irregular geometry. Int J Solid Struct 2007;44:5576–97.
18. Piccardo G, Tubino F, Luongo A. Equivalent timoshenko linear beam model for the static and dynamic analysis of tower buildings. Appl Math Model 2019;71:77–95.
19. Firouzbakhsh J, Malekinejad M, Rahgozar R. Reducing the cost of calculations for stability analysis of tall buildings using a new approach. Lat Am J Solid Struct 2024;21:e558.
20. Pinto-Cruz MC. Static, dynamic, and stability analysis of coupled shear walls: correction factors due to local shear deformation of the walls. Structures 2025;75:108754.
21. Carpinteri A, Lacidogna G, Puzzi S. A global approach for three-dimensional analysis of tall buildings. Struct Des Tall Special Build 2010; 19:518–36.
22. Carpinteri A, Corrado M, Lacidogna G, Cammarano S. Lateral load effects on tall shear wall structures of different height. Struct Eng Mech 2012;41:313–37.
23. Gong J, Fang T, Zuo J. A review of key technologies development of super high-rise building construction in China. Adv Civ Eng 2022;2022: 5438917.
24. Li Q, Wang L. Is the Chinese skyscraper boom excessive? J Urban Aff 2022;44:1117–35.
25. Al-Kodmany K. Constructing tall buildings in China: with a focus on Shanghai. Int J High-Rise Buildings 2024;13:33–56.
26. Yuan T, Chen S, Liu S, Lu X. Influence of tall buildings on city-scale seismic response analysis: a case study of Shanghai CBD. Soil Dynam Earthq Eng 2023;173:108063.
27. Cheng X, Huang G, Yang Q, Zhou X. Influence of architectural facades on wind pressures and aerodynamic forces of tall buildings. J Struct Eng 2021;147:04020303.
28. Nematchoua MK, Asadi S, Reiter S. Estimation, analysis and comparison of carbon emissions and construction cost of the two tallest buildings located in United States and China. Int J Environ Sci Technol 2022;19: 9313–28.
29. Gui C, Yan D, Hong T, Xiao C, Guo S, Tao Y. Vertical meteorological patterns and their impact on the energy demand of tall buildings. Energy Build 2021;232:110624.
30. Capurso M. Sul calcolo dei sistemi spaziali di controventamento, parte 1. Giornale Del Genio Civile 1981;1-2-3:27–42.
31. Carpinteri A, Carpinteri A. Lateral loading distribution between the elements of a three-dimensional civil structure. Comput Struct 1985;21: 563–80.
32. Carpinteri A, Lacidogna G, Nitti G. Open and closed shear-walls in high-rise structural systems: static and dynamic analysis. Curved Layer Struct 2016;3. https://doi.org/10.1515/cls-2016-0013.
33. Nitti G, Lacidogna G, Carpinteri A. An analytical formulation to evaluate natural frequencies and mode shapes of high-rise buildings. Curved Layer Struct 2021;8:307–18.
34. Zalka KA. A simplified method for calculation of the natural frequencies of wall–frame buildings. Eng Struct 2001;23:1544–55.
35. Ali MM, Sun Moon K. Advances in structural systems for tall buildings: emerging developments for contemporary urban giants. Buildings 2018;8:104.
36. V Zakharovich Vlasov, *Thin-walled elastic beams*, 2d ed. rev. and augm. translated from russian [by y. schectman] ed., Jerusalem : Published for the National Science Foundation, Washington, D.C., by the Israel Program for Scientific Translations, Jerusalem (Israel)-place of publication, 1961 [available from the Office of Technical Services, U.S. Dept of Commerce, Washington].